Lattice-Charge Coupling in a Trilayer Nickelate with Intertwined Density Wave Order

Xun Jia,[1,2,*] Yao Shen,[3,†] Harrison LaBollita,[4,‡] Xinglong Chen,[1,§] Junjie Zhang,[1,‖] Yu Li,[1] Hengdi Zhao,[1] Mercouri G. Kanatzidis,[1,5] Matthew Krogstad,[6] Hong Zheng,[1] Ayman H. Said,[6] Ahmet Alatas,[6] Stephan Rosenkranz,[1] Daniel Phelan,[1] Mark P. M. Dean,[3,7] M. R. Norman,[1] J. F. Mitchell,[1] Antia S. Botana,[4,¶] and Yue Cao[1,**]

[1]*Materials Science Division, Argonne National Laboratory, Lemont, Illinois 60439, USA*
[2]*Multi-disciplinary Research Division, Institute of High Energy Physics, Chinese Academy of Sciences, Beijing 100049, China*
[3]*Condensed Matter Physics and Materials Science Department, Brookhaven National Laboratory, Upton, New York 11973, USA*
[4]*Department of Physics and Astronomy, Arizona State University, Tempe, Arizona 85218, USA*
[5]*Department of Chemistry, Northwestern University, Evanston, Illinois 60208, USA*
[6]*X-ray Science Division, Argonne National Laboratory, Lemont, IIllinois 60439, USA*
[7]*Department of Physics and Astronomy, The University of Tennessee, Knoxville, Tennessee 37966, USA*

(Received 10 July 2025; revised 9 November 2025; accepted 9 December 2025; published 23 January 2026)

Intertwined charge and spin correlations are ubiquitous in a wide range of transition metal oxides and are often perceived as intimately related to unconventional superconductivity. Theoretically envisioned as driven by strong electronic correlations, the intertwined order is usually found to be strongly coupled to the lattice as signaled by pronounced phonon softening. Recently, both charge and spin density waves (CDW and SDW) and superconductivity have been discovered in several Ruddlesden-Popper (RP) nickelates, in particular trilayer nickelates $RE_4Ni_3O_{10}$ (RE = Pr, La). The nature of the intertwined order and the role of lattice-charge coupling are at the heart of the debate about these materials. Using inelastic x-ray scattering, we mapped the low-energy phonon dispersions in $RE_4Ni_3O_{10}$ and found no evidence of softening near the CDW wave vector over a wide temperature range, which contrasts with the pronounced anomalies frequently observed in cuprate superconductors. Calculations of the electronic susceptibility revealed a peak at the observed SDW ordering vector but not at the CDW wave vector. Our experimental and theoretical findings highlight the crucial role of the spin degree of freedom and establish a foundation for understanding the interplay between superconductivity and density-wave transitions in RP nickelate superconductors and beyond.

DOI: 10.1103/s5j9-cbg7

Subject Areas: Condensed Matter Physics, Strongly Correlated Materials, Superconductivity

I. INTRODUCTION

Intertwined charge and spin density waves (CDW and SDW) refer to a quantum phase of matter where strong electronic correlations induce cooperation rather than competition between the charge and spin degrees of freedom [1,2]. In transition metal oxides, such intertwined order often coexists or resides in the vicinity of unconventional superconductivity. While initially proposed theoretically as an electronic phase of matter, the nature of the intertwined order remains enigmatic in transition metal oxides, especially regarding its interaction with the underlying lattice. Experimentally, the onset of intertwined CDW/SDW order is almost invariably accompanied by sizable distortions of the lattice. These lattice deformations manifest as temperature-dependent phonon dispersion anomalies near the wave vector of the charge order, which were observed prominently across different families of the canonical high T_c cuprates [3–7]. These pronounced

*Contact author: jiaxun@ihep.ac.cn
†Present address: Institute of Physics, Chinese Academy of Sciences, Beijing 100190, China.
‡Present address: Center for Computational Quantum Physics, Flatiron Institute, New York, New York 10010, USA.
§Present address: School of Physics, Southeast University, Nanjing, 211189, China.
‖Institute of Crystal Materials, State Key Laboratory of Crystal Materials, Shandong University, Jinan, Shandong 250100, China.
¶Contact author: antia.botana@asu.edu
**Contact author: yue.cao@anl.gov

phonon anomalies appear not only in the higher-energy bond stretching modes but also in the lower-energy branches. Despite extensive studies, whether strong electron-phonon coupling is universal or essential in correlated oxide superconductors, cuprates or otherwise, remains elusive.

The discovery of superconductivity in valence-reduced Ruddlesden-Popper (RP) nickelates [8,9] and more recently in the RP nickelates themselves [10–17] provides new opportunities for understanding the nature of intertwined order. To date, no robust signatures of spin and charge order occur in infinite-layer nickelates [18–21], although both are present in reduced trilayer nickelates [22]. Both spin and charge order were discovered in the bilayer RP nickelate $La_3Ni_2O_7$ [23,24] and diminished under pressure before the emergence of superconductivity. $RE_4Ni_3O_{10}$ (RE = Pr, La) are among the latest additions to the superconducting nickelates under pressure [12,13,17], with a number of electronic properties resembling the cuprates [14]. The presence of intertwined CDW/SDW order in the trilayer RP nickelates was previously elucidated by elastic x-ray and neutron diffraction [25,26]. These experimental findings would suggest strong lattice deformations similar to those observed in cuprates.

Here, we show phonon dispersions in a range of energies near the CDW ordering vector in $RE_4Ni_3O_{10}$ and demonstrate the surprising absence of phonon anomalies or softening over a wide temperature range using inelastic x-ray scattering (IXS). Calculations of the susceptibility based on the paramagnetic electronic structure reveal a nesting instability at the SDW ordering vector but not at the CDW one. Our observations suggest a leading role of spin in the transition to the density wave state in the trilayer nickelates, with a relatively minor connection to lattice deformations.

II. RESULTS

A. Temperature dependence of the intertwined density waves

$RE_4Ni_3O_{10}$ is the $n = 3$ member of the RP series and features three layers of corner-sharing NiO_6 octahedra [Figs. 1(a) and 1(c)]. Similar to some 214 cuprates, the NiO_6 octahedra rotate relative to the c axis by 10.9° for $Pr_4Ni_3O_{10}$ and 6.84° for $La_4Ni_3O_{10}$ towards the b axis, leading to an in-plane Ni—O—Ni bond angle of 157.3° for $Pr_4Ni_3O_{10}$ and 166.6° for $La_4Ni_3O_{10}$. These octahedral tilts give rise in both $Pr_4Ni_3O_{10}$ and $La_4Ni_3O_{10}$ to the monoclinic $P2_1/a$ space group [Fig. 1(c)] [22,27]. In terms of the electronic structure, the Ni site has an average valence of $Ni^{2.67+}$ with a $3d^{7.33}$ configuration. Thus, analogous to commensurately doped cuprates [28], nickelates [29], and manganites [30], the Ni valence would be expected to favor a site-by-site variation of the Ni valence, nominally Ni^{3+}-Ni^{2+}-Ni^{3+}, that would be stabilized by commensurate deformations of the underlying lattice.

Deviating from these expectations, intertwined CDW/SDW order exists in both $La_4Ni_3O_{10}$ and $Pr_4Ni_3O_{10}$ [25,26], with in-plane ordering wave vectors significantly different from the above expectation. For $Pr_4Ni_3O_{10}$, the in-plane SDW and CDW wave vectors are $(0\,0.61)$ and $(0\,0.78)$, respectively, well away from the anticipated value of $(0\,2/3)$ for both. The selection rules of the two order parameters are displayed in Fig. 1(b). We adopt the unit cell for the monoclinic $P2_1/a$ space group, while previous studies have used the pseudo-orthorhombic notation ($Bmab$) to account for the twinning of crystallographic domains (the deviation of $P2_1/a$ from $Bmab$ is small). Hereafter, for clarity, we will use the subscripts o and m to distinguish the Miller indices under the two notations,

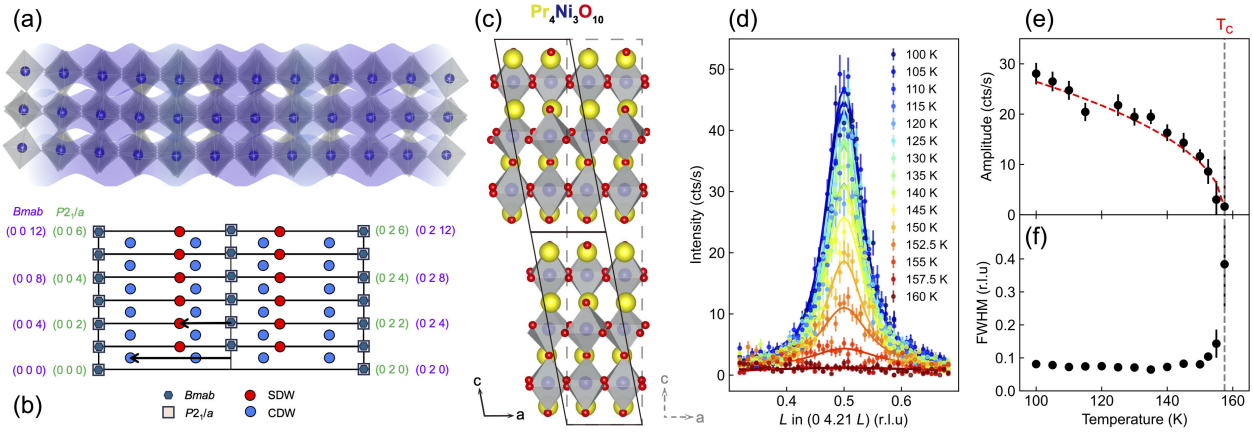

FIG. 1. Intertwined spin and charge density wave order in $Pr_4Ni_3O_{10}$. (a) Illustration of the charge density wave. The gray shading illustrates the charge density distribution. (b) Schematic of the $0kl$ plane showing the location of $Bmab$ and $P2_1/a$ fundamentals and both CDW and SDW superlattice reflections. (c) Crystal structure of $Pr_4Ni_3O_{10}$. The unit cell contains three layers of corner-sharing NiO_6 octahedra that are related by an approximate B-centering operation with the $P2_1/a$ unit cells shown by black solid lines and the related pseudo-orthorhombic unit cell by gray dashed lines. (d), (e) Temperature evolution of the charge density wave order $—(0\,4.21\,0.5)_m$. (d) Temperature dependence of an L scan through the CDW peak with (e), (f) showing the fitted amplitude and FWHM of this order, respectively.

with the correspondence between the two notations given by $(H\,K\,L)_o \equiv (H\,K\,L/2 - H/2)_m$. Unless otherwise stated, all the data and calculations in the main text concern $Pr_4Ni_3O_{10}$. Results for $La_4Ni_3O_{10}$ can be found in Ref. [31].

In Fig. 1(d), we present the temperature dependence of the elastic data at one of these CDW wave vectors $\boldsymbol{Q}_{\mathrm{CDW}} = (0\,4.21\,0.5)_m$. The diffraction intensity was obtained using an IXS spectrometer with an energy resolution of 1.36 meV [32]. Further experimental details are presented in the Methods. The evolution of the diffraction intensity and the full width at half maximum (FHWM) of the CDW order with temperature are in Figs. 1(e) and 1(f), respectively. The onset of the CDW is at $T_{\mathrm{CDW}} \sim 157.5$ K, consistent with previous findings [25,26]. At the lowest temperature of 10 K in our measurement, the FWHM of the CDW order is 0.075 r.l.u. corresponding to a correlation length of approximately 6 nm along the c axis. Fitting the temperature-dependent amplitude using a functional form of $(1 - T/T_{\mathrm{CDW}})^n$ yields a critical exponent $n \sim 0.46$ close to the mean-field value of 0.5. Nominally, this critical index is consistent with a second-order phase transition. However, competing experimental observations and theoretical analysis suggest that the phase transition is weakly first order [27,33]. To add to the complexity, in previous studies [25,26], the critical exponent for the SDW order is essentially identical to that of the CDW, which would suggest that both the CDW and SDW are primary order parameters. In comparison, in commensurately doped cuprates [28], the critical exponent of the charge order is smaller than that of the spin order. Beyond strongly correlated oxides, for chromium, an established CDW/SDW material, the CDW order is secondary with a critical exponent twice that of the SDW [34]. Thus, examining the charge order in more detail should provide crucial insights into the nature of the intertwined CDW/SDW and the potential role of electron-phonon coupling in the trilayer nickelates.

B. Persistent phonon dispersions near the CDW wave vector

We performed nonresonant IXS to understand the electron-phonon coupling in $RE_4Ni_3O_{10}$, focusing on the lower energy phonon branches that are accessible by this technique. Figures 2(a) and 2(b) show the measured phonon spectra between $(0\,4\,0.5)_m$ and $(0\,4.5\,0.5)_m$ at 100 K (below T_{CDW}) and at 300 K (above T_{CDW}), respectively. This cut in reciprocal space was chosen for its relatively strong CDW peak intensity and for its large inelastic phonon scattering cross section. Up to four phonon branches are distinguishable and are marked using white solid circles.

The CDW ordering wave vector $\boldsymbol{Q}_{\mathrm{CDW}}$ is marked using a vertical dashed line, with pronounced elastic scattering intensity at 100 K, demonstrating the presence of charge order. The temperature dependence of the elastic scattering from the CDW order is presented in Figs. 1(c)–1(e) as noted above. The measured phonon dispersions and spectral weights do not change across the phase transition within our experimental resolution, with no discernible phonon softening at $\boldsymbol{Q}_{\mathrm{CDW}}$. Notably, in monoclinic notation, the CDW wave vector has an out-of-plane component of $L = 0.5$. As such, $\boldsymbol{Q}_{\mathrm{CDW}}$ is away from any high symmetry direction of the Brillouin zone. As a result, at $(0\,4\,0.5)_m$, the observed phonon energies remain finite. More importantly, the eigenvectors corresponding to the observed phonon modes cannot be simply characterized as longitudinal or transverse. This actually reduces the possibility that the lattice deformation responsible for the CDW is completely orthogonal to the phonon modes we captured and hence escaped detection.

To delve into this further, we calculated the phonon dispersions using the phonon density functional theory (PDFT) [Fig. 2(c)]. Details of the PDFT are in the Methods. The calculated phonon dispersions agree to the most part with the experimental results, especially near $(0\,4\,0.5)_m$. There is a larger discrepancy for the highest phonon branch near $(0\,4.5\,0.5)_m$. This most likely arises from the large number of phonon branches due to the low monoclinic symmetry and an energy-varying phonon spectral weight in the IXS measurements.

The absence of a Kohn anomaly in any of these phonon branches is striking. In comparison, a phonon softening of 2 meV is seen in $La_{1.875}Ba_{0.125}CuO_4$ [7] and as high as 5 meV in $YBa_2Cu_3O_{6.6}$ [6] for phonons in a similar energy range, though only one of the two detected branches softened in [7] while both softened in [6]. The softened phonon branches should, in principle, have atomic displacements relevant to the formation of the CDW. To this end, we calculated the eigenvectors of the measured phonon branches, encompassing ionic motions both in and out of the Ni-O planes. In Figs. 2(d) and 2(e), we show the calculated eigenvectors in the monoclinic unit cell for two of these phonon branches. For the lowest-lying branch, the Ni and O atoms predominantly vibrate along the a axis and with a significant shearing between the center Ni-O plane and the outer ones [Fig. 2(d)]. The higher-energy mode corresponds to a superposition of the breathing of the apical oxygens and an octahedral rotation relative to the Ni-O planes. There are also large A-site displacements for the eigenvectors of all four phonon branches we could observe, and none along any high symmetry direction. This reduces the possibility that the phonon softening was not observed for symmetry reasons. In other correlated oxides, these deformations of the metal-oxygen octahedra help stabilize charge order. Therefore, since the four phonon modes we could resolve should include vibrations affected by the CDW order, the lack of any softening is striking.

To rule out phonon softening at Q_{CDW}, we track the detailed temperature dependence of the phonon dispersions. Figures 3(a) and 3(b) depict the IXS spectra

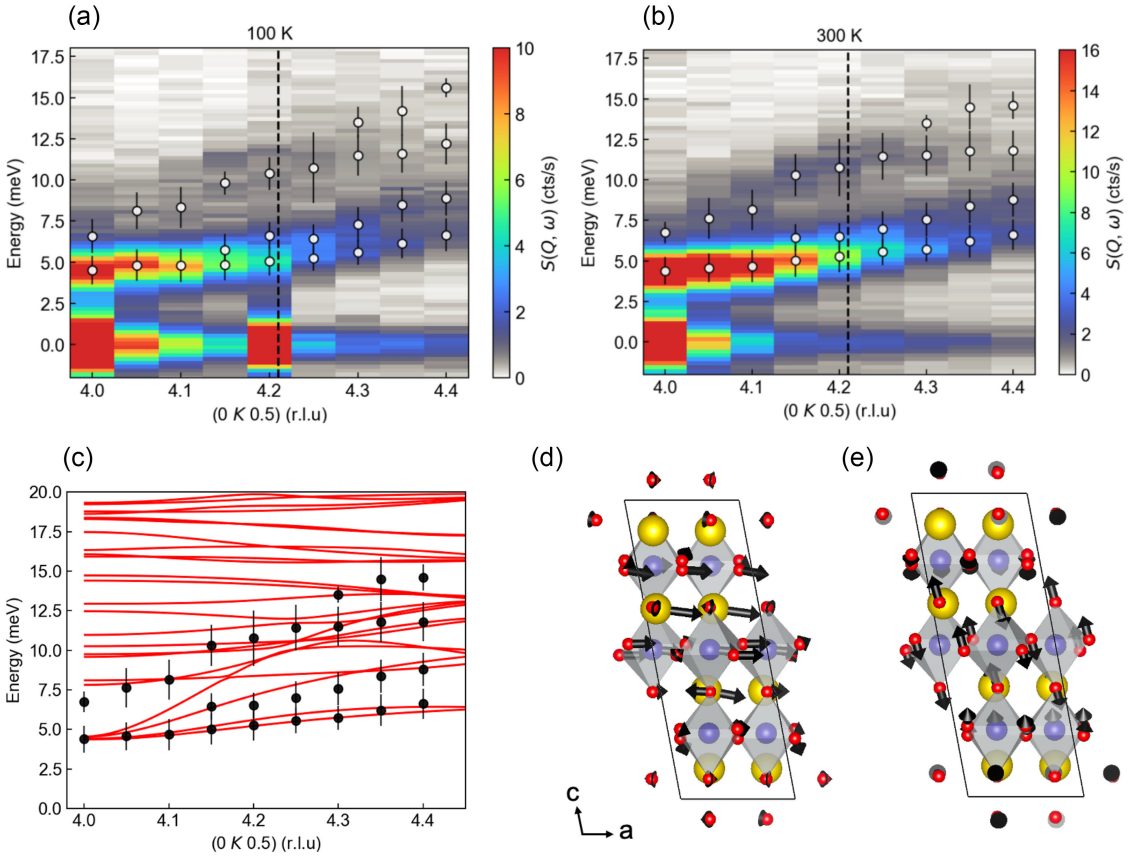

FIG. 2. Phonon dispersions below and above T_{CDW} and the eigenvectors of the phonon modes near the charge density wave order $(0\,4.21\,0.5)_m$. (a) and (b) 2D map of the phonon dispersions at 100 and 300 K, respectively. The black empty circles correspond to the energy of the phonon modes and the vertical bars to their peak widths. The vertical dashed line marks the CDW wave vector. (c) Calculated phonon dispersions (solid red curves) with the fitting results from experiments (solid black circles with error bars). (d) and (e) Eigenvectors of the phonons with energies of 5.28 and 7.31 meV at the CDW wave vector.

at $(0\,4.2\,0.5)_m$ and $(0\,4.25\,0.5)_m$. Among the two, $(0\,4.2\,0.5)_m$ is essentially at $\boldsymbol{Q}_{\mathrm{CDW}}$, with a separation well within the FWHM of the CDW wave vector. The elastic spectral weight increases below $\mathrm{T_{CDW}}$ following the onset of the order parameter. Fitting procedures identical to those in Fig. 2 were used, with the contribution from each branch shown as shaded areas underneath the corresponding phonon spectra. For the two momentum transfers shown in Fig. 3, consistent with Fig. 2, three phonon branches were used to optimize the fit.

The energy and the FWHM of the three phonon branches are displaced in Figs. 3(c) and 3(d) for $(0\,4.2\,0.5)_m$ and $(0\,4.25\,0.5)_m$ respectively, which are essentially unchanged. Indeed, no change in the phonon dispersions was observed along the entire $(0\,\mathrm{K}\,0.5)_m$ cut. Further discussion about the temperature evolution can be found in Ref. [31].

C. The role of SDW on the emergence of the intertwined order

The absence of any phonon anomalies at or near $\boldsymbol{Q}_{\mathrm{CDW}}$ is highly nontrivial. It begs the question of whether any phonon softening occurs in the material, and if it does, where in energy and in reciprocal space this would occur and how much softening would be present. For instance, large phonon anomalies were seen in optical branches at much higher energies in both cuprates and 214 nickelates [35,36]. Unfortunately, our IXS setup does not allow enough scattered x-ray photons to study these high-energy phonons. Nonetheless, as demonstrated earlier in the paper, our observation is dramatically different from other correlated oxides where the robust charge order is associated with insulating-like behavior. Instead, in the 4310 nickelates, the intertwined order is associated with a metal-metal transition, similar to what is observed in chromium.

Therefore, a more likely scenario has to do with the unique electronic structure of the trilayer nickelates. To demonstrate the relation of the CDW/SDW to the electronic structure, we examine the potential role of Fermi surface nesting by calculating the bare susceptibility function

$$\chi_0(\boldsymbol{Q}) = 2\sum_{n,n'} \int d\boldsymbol{k} \frac{f_{\boldsymbol{k}+\boldsymbol{Q},n'} - f_{\boldsymbol{k},n}}{\epsilon_{\boldsymbol{k}+\boldsymbol{Q},n'} - \epsilon_{\boldsymbol{k},n}}, \tag{1}$$

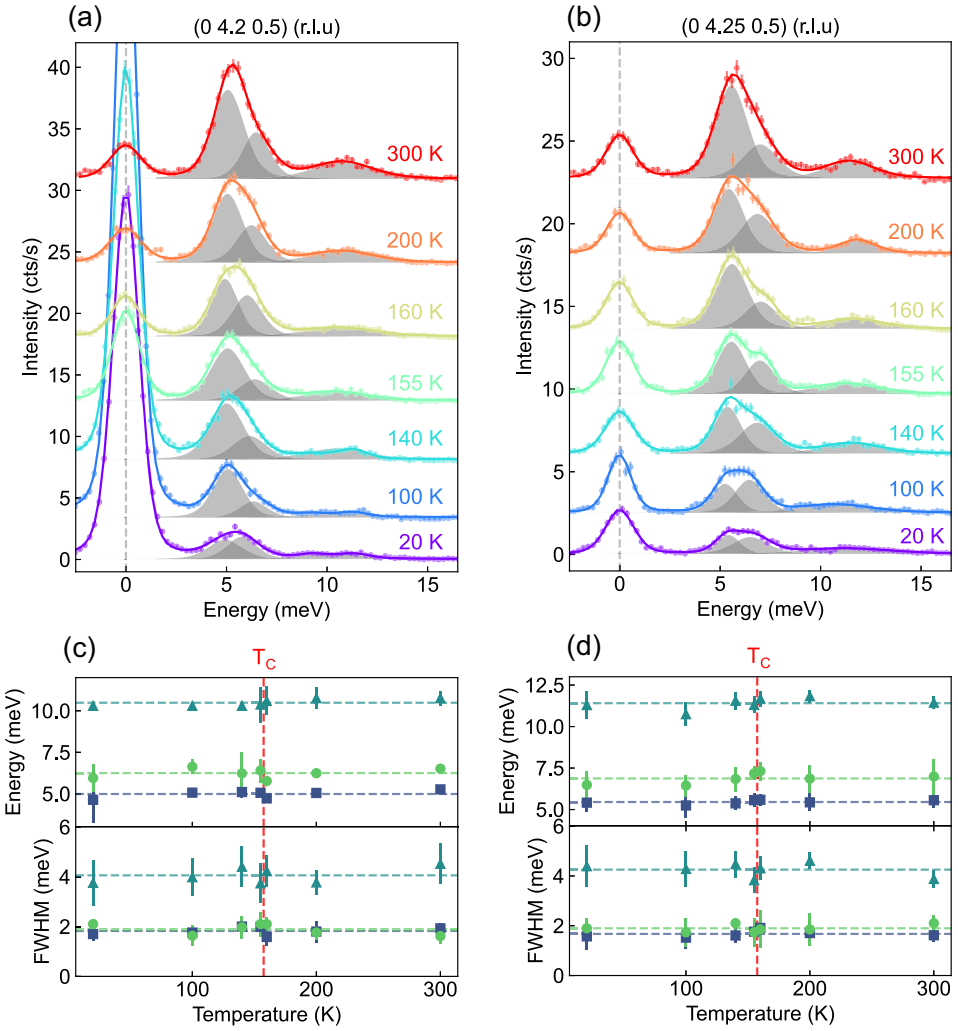

FIG. 3. Temperature-dependent phonon line shape analysis around the CDW wave vector. (a) and (b) Temperature dependence of the constant-$\boldsymbol{Q}$ phonon measurements at $\boldsymbol{Q} = (0\,4.20\,0.5)_m$ and $(0\,4.25\,0.5)_m$, respectively. The phonons, fitted as shown by the gray shading, are observed by meV-resolved inelastic x-ray scattering. (c) and (d) Temperature dependence of the fitted energy positions and FWHMs of the phonons at $\boldsymbol{Q} = (0\,4.20\,0.5)_m$ and $(0\,4.25\,0.5)_m$, respectively. The red dashed lines mark T_{CDW}.

with the full χ given by $\chi_0/[1 - I\chi_0(\boldsymbol{Q})]$, where I is the interaction associated with the order (the denominator of χ going to zero marks the onset of mean-field order). Here f is the Fermi function and ϵ are the band energies with n,n' band indices. The factor of 2 takes into account the sum over spin. For $La_4Ni_3O_{10}$, the band structure and susceptibility were calculated previously using the orthorhombic *Bmab* structure [25]. One issue with that calculation was the neglect of matrix elements in Eq. (1) (that is, of the band wave functions with the change or spin operators). This effect can be mitigated by using an unfolded Brillouin zone [37]. Therefore, we calculated the band structure and the corresponding Fermi surface of $Pr_4Ni_3O_{10}$ using the tetragonal $I4/mmm$ unfolded structure [Figs. 4(a) and 4(b)]. As shown in Fig. 4(b), the large electron pocket centered around Γ can be connected to the two large hole pockets centered around M by a vector equal to the observed SDW ordering vector, while we observe no obvious nesting at the observed CDW vector. This is confirmed by calculations of $\chi_0(\boldsymbol{Q})$ [Figs. 4(c) and 4(d)], where a peak in χ_0 is obtained at the observed SDW vector, which can be attributed to the interband terms referred to above, with no peak observed at the CDW wave vector.

The presence of a susceptibility peak at $\boldsymbol{Q}_{\mathrm{SDW}}$ demonstrates that spin rather than charge is the driving force behind the onset of the intertwined order. This calculation is consistent with the absence of a Kohn anomaly in our data at the CDW wave vector. In principle, phonon softening could be present at the SDW wave vector as observed in chromium [38]. However, IXS data we have taken at one of the SDW ordering vectors also found no evidence for phonon softening [31]. Such an observation further establishes the critical role of the spin degree of freedom. We further comment on the temperature dependence of the

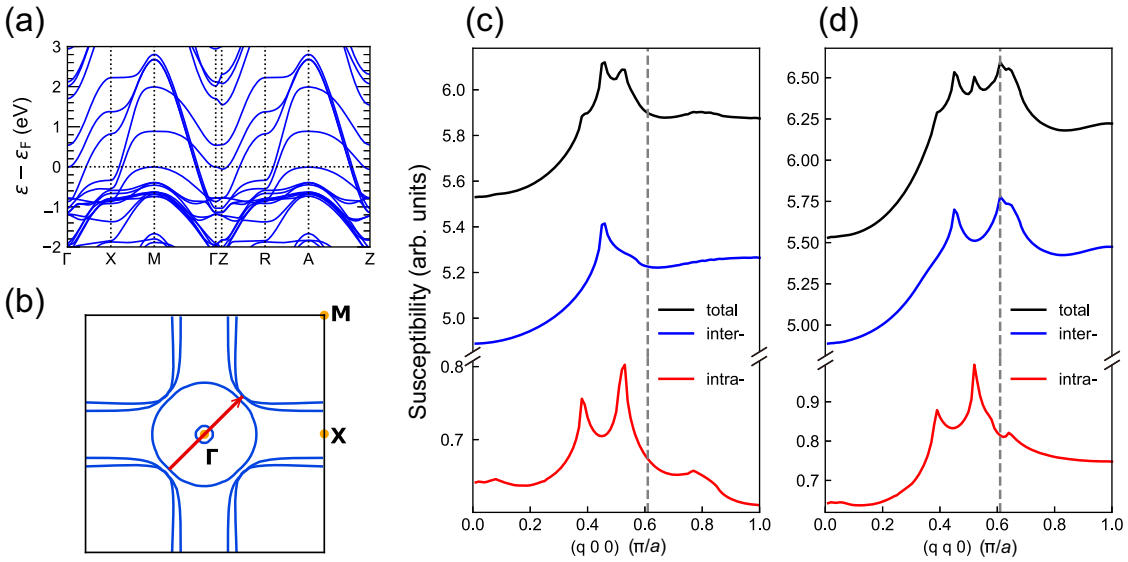

FIG. 4. The origin of the SDW order in $Pr_4Ni_3O_{10}$. (a) Band structure of $Pr_4Ni_3O_{10}$ along high symmetry cuts in the tetragonal $I4/mmm$ zone. (b) Fermi surface contours of $Pr_4Ni_3O_{10}$ with the nesting vector indicated in red. (c) and (d) Susceptibility showing the total contribution, interband contribution, and intraband contribution along $(q\,0\,0)$ and $(q\,q\,0)$, respectively, with the observed SDW wave vector indicated by the vertical dashed line in (d). The predicted order occurs along the zone diagonal at the observed SDW wave vector $(0.61\,0.61\,0)$ in tetragonal notation (the L dependence, due to magnetic coupling between layers, is not captured by χ_0). No structure is seen at the observed CDW wave vector.

SDW and CDW order parameters [Fig. 1]. That both order parameters share similar critical exponents may be a result of the intertwined order being proximate to a first-order transition. Details can be found in [33].

The temperature independence of the phonon dispersions is unusual not only among correlated oxides, but even compared to CDW and SDW materials with weaker electronic correlations. For example, the CDW in transition metal dichalcogenides such as 2H-$NbSe_2$ were initially perceived as driven by the electronic structure. However, in the majority of these dichalcogenides, phonons soften and become overdamped substantially when cooling down towards the CDW phase transition, e.g., by ∼8 meV in 2H-$NbSe_2$ [39], followed by the expected hardening below the phase transition. Similarly for Cr, phonons soften as a function of temperature not only at the SDW wave vector, but over extended regions of the zone boundary in reciprocal space [38].

The significance of our findings is highlighted in the much stronger electron correlations compared to the aforementioned dichalcogenides. Indeed, the intertwined order in $RE_4Ni_3O_{10}$ presents an intriguing case for an electronically driven intertwined order with weak coupling to the lattice, closer to the original theoretical proposals than many of the more studied oxides. Thus, the trilayer nickelates could provide a much-sought-after playground for understanding the emergent properties of such states.

III. CONCLUSION

The unaltered-with-temperature phonon dispersions in the trilayer nickelates that we observed are markedly different from those in other correlated oxides and potentially represent a new regime of intertwined order stabilized by the strong interaction of the spin degree of freedom and associated with a metal-metal transition. Fully elucidating the role of the lattice in the formation of the CDW/SDW requires further experimental and theoretical efforts, including a three-dimensional refinement of any potential lattice distortions associated with the phase transition, as well as calculations of the electron-phonon coupling across the entire Brillouin zone. Nonetheless, the new regime we discovered provides a valuable playground both for understanding the nature of the electronically intertwined order weakly coupled to the lattice. Since non-conventional superconductivity has been reported in trilayer RP nickelates, our findings lay the groundwork for revealing the cooperative vs competing relationship between the intertwined order and superconductivity in and beyond nickelates.

IV. METHODS

A. Material synthesis and sample preparation

$Pr_4Ni_3O_{10}$ crystals were grown in a high-pressure optical floating zone furnace (HKZ 150-bar Model, ScIDre, Germany) [27,40]. Stoichiometric Pr_6O_{11} and NiO powders were thoroughly mixed and sintered at 1050 °C for 36 h with several intermediate grindings to obtain the precursor powder of $Pr_4Ni_3O_{10}$. Precursor powder was pressed into a rod with a diameter of ∼6 mm by hydrostatic press and then sintered for 24 h at 1050 °C. $Pr_4Ni_3O_{10}$ crystals were grown via a two-step method at an oxygen

pressure of 140 bar using a 5 kW xenon lamp as the heating source: The first step was a fast pass and melt with a traveling rate of 30–50 mm/h to obtain a rod with improved density, and the second step was the slow growth using the densified rod with a traveling rate of 4–5 mm/h. During the growth, the feed and seed rods were counter-rotated at 15–25 rpm, and an oxygen flow rate of 0.1 L/min was maintained. Single crystals were mechanically separated from the as-grown boule.

Single crystals were aligned using a lab-based four-circle x-ray diffractometer with a photon energy of 8.05 keV at room temperature to confirm the crystal is in pure $P2_1/a$ phase. To meet the experimental requirements of inelastic x-ray scattering and have good statistics from inelastic scattering signals, the crystal was further polished with the thickness down to around 150 μm.

B. Inelastic x-ray scattering

The inelastic x-ray scattering experiment was performed at beamline 30-ID-C (HERIX) of the Advanced Photon Source. The highly monochromatic x-ray beam with an incident energy of 23.7 keV was focused on the sample with a cross section of $\sim 35 \times 15\ \mu m^2$ (horizontal × vertical). The total energy resolution of the monochromatic x-ray beam and analyzer crystals was $\Delta E \sim 1.36$ meV (FWHM) [31]. The phonon measurements were performed in the Laue geometry, while the diffraction was performed in transmission geometry. Typical counting times ranged from 30 sec to 1 min per point in the energy scans at constant momentum transfer Q.

C. X-ray diffraction

Single crystal x-ray diffraction measurements were performed at the beamline 15-ID-D at ChemMatCARS (University of Chicago) of the Advanced Photon Source, Argonne National Laboratory [25,31]. The experiment was carried out with 30 keV x-ray photons ($\lambda = 0.413$ Å) and the diffracted x rays were collected with a Pilatus 1M area detector.

D. Phonon density functional theory calculations

The phonon spectrum of $Pr_4Ni_3O_{10}$ ($P2_1/a$) is computed from first-principles using the frozen phonon method as implemented in phonopy interfaced with VASP [41,42]. We employed the Perdew-Burke-Ernzerhof exchange-correlation functional [43], a plane-wave energy cutoff of 500 eV, and a Gamma-centered $2 \times 8 \times 8$ k-mesh with 0.1 eV Gaussian smearing.

E. Susceptibility calculations

Equation (1) is written in the approximation that matrix elements between the band wave functions and the charge or spin operators are not accounted for. In such an approximation, it is best to use an unfolded Brillouin zone [37]. Hence, we compute the band structure of $Pr_4Ni_3O_{10}$ for the high-symmetry tetragonal ($I4/mmm$) structure using the all-electron, full potential DFT code WIEN2K [44] with the PBE exchange-correlation functional. The basis set size was set by $RK_{max} = 7$ and $R_{MT} = 2.37$, 1.90, and 1.69 for Pr, Ni, and O, respectively. Brillouin zone integrations were done on a $21 \times 21 \times 21$ k-mesh. The Pr($4f$) electrons are treated as core electrons within the open-core approximation.

To calculate the static bare susceptibility $\chi_0(\vec{Q})$, we interpolate the five bands nearest the Fermi energy using a Fourier spline series [45], with 2436 functions fit to 726 k points in the irreducible wedge of the Brillouin zone. Equation (1) was then evaluated using a tetrahedron decomposition of the Brillouin zone (3×8^5 tetrahedra in the irreducible wedge) [46].

ACKNOWLEDGMENTS

The sample synthesis, IXS measurements, data analysis, and susceptibility calculations at Argonne National Laboratory were supported by the U.S. Department of Energy, Office of Science, Basic Energy Sciences, Materials Science and Engineering Division. Work at Brookhaven (x-ray scattering and data interpretation by Y. S. and M. P. M. D.) was supported by the U.S. Department of Energy, Office of Science, Office of Basic Energy Sciences, under Award No. DE-SC0022311. A. S. B. and H. L. acknowledge support from NSF Grant No. DMR-2045826 and from the ASU research computing center for HPC resources. This research used resources of the Advanced Photon Source (APS), with some of the data collected via APS beam time award (10.46936/APS-189700/60013854). The APS is a U.S. Department of Energy (DOE) Office of Science user facility operated by Argonne National Laboratory under Contract No. DE-AC02-06CH11357.

DATA AVAILABILITY

The data are not publicly available. The data are available from the authors upon reasonable request.

[1] E. Fradkin, S. A. Kivelson, and J. M. Tranquada, *Colloquium: Theory of intertwined orders in high temperature superconductors*, Rev. Mod. Phys. **87**, 457 (2015).

[2] D. F. Agterberg, J. S. Davis, S. D. Edkins, E. Fradkin, D. J. Van Harlingen, S. A. Kivelson, P. A. Lee, L. Radzihovsky, J. M. Tranquada, and Y. Wang, *The physics of pair-density waves: Cuprate superconductors and beyond*, Annu. Rev. Condens. Matter Phys. **11**, 231 (2020).

[3] R. J. McQueeney, Y. Petrov, T. Egami, M. Yethiraj, G. Shirane, and Y. Endoh, *Anomalous dispersion of lo phonons in* $La_{1.85}Sr_{0.15}CuO_4$ *at low temperatures*, Phys. Rev. Lett. **82**, 628 (1999).

[4] D. Reznik, L. Pintschovius, M. Ito, S. Iikubo, M. Sato, H. Goka, M. Fujita, K. Yamada, G. Gu, and J. Tranquada, *Electron–phonon coupling reflecting dynamic charge inhomogeneity in copper oxide superconductors*, Nature (London) **440**, 1170 (2006).

[5] A. Q. Baron, J. P. Sutter, S. Tsutsui, H. Uchiyama, T. Masui, S. Tajima, R. Heid, and K.-P. Bohnen, *First study of the* B_{1g} *buckling phonon mode in optimally doped, de-twinned,* $YBa_2Cu_3O_{7-\delta}$ *by inelastic X-ray scattering*, J. Phys. Chem. Solids **69**, 3100 (2008).

[6] M. Le Tacon, A. Bosak, S. Souliou, G. Dellea, T. Loew, R. Heid, K. Bohnen, G. Ghiringhelli, M. Krisch, and B. Keimer, *Inelastic x-ray scattering in* $YBa_2Cu_3O_{6.6}$ *reveals giant phonon anomalies and elastic central peak due to charge-density-wave formation*, Nat. Phys. **10**, 52 (2014).

[7] H. Miao, D. Ishikawa, R. Heid, M. Le Tacon, G. Fabbris, D. Meyers, G. D. Gu, A. Q. R. Baron, and M. P. M. Dean, *Incommensurate phonon anomaly and the nature of charge density waves in cuprates*, Phys. Rev. X **8**, 011008 (2018).

[8] D. Li, K. Lee, B. Y. Wang, M. Osada, S. Crossley, H. R. Lee, Y. Cui, Y. Hikita, and H. Y. Hwang, *Superconductivity in an infinite-layer nickelate*, Nature (London) **572**, 624 (2019).

[9] G. A. Pan, D. Ferenc Segedin, H. LaBollita, Q. Song, E. M. Nica, B. H. Goodge, A. T. Pierce, S. Doyle, S. Novakov, D. Córdova Carrizales *et al.*, *Superconductivity in a quintuple-layer square-planar nickelate*, Nat. Mater. **21**, 160 (2022).

[10] H. Sun, M. Huo, X. Hu, J. Li, Z. Liu, Y. Han, L. Tang, Z. Mao, P. Yang, B. Wang *et al.*, *Signatures of superconductivity near 80 K in a nickelate under high pressure*, Nature (London) **621**, 493 (2023).

[11] X. Chen, J. Choi, Z. Jiang, J. Mei, K. Jiang, J. Li, S. Agrestini, M. Garcia-Fernandez, H. Sun, X. Huang *et al.*, *Electronic and magnetic excitations in* $La_3Ni_2O_7$, Nat. Commun. **15**, 9597 (2024).

[12] Y. Zhu, D. Peng, E. Zhang, B. Pan, X. Chen, L. Chen, H. Ren, F. Liu, Y. Hao, N. Li *et al.*, *Superconductivity in pressurized trilayer* $La_4Ni_3O_{10-\delta}$ *single crystals*, Nature (London) **631**, 531 (2024).

[13] M. Zhang *et al.*, *Superconductivity in trilayer nickelate* $La_4Ni_3O_{10}$ *under pressure*, Phys. Rev. X **15**, 021005 (2025).

[14] Q. Li, Y.-J. Zhang, Z.-N. Xiang, Y. Zhang, X. Zhu, and H.-H. Wen, *Signature of superconductivity in pressurized* $La_4Ni_3O_{10}$, Chin. Phys. Lett. **41**, 017401 (2024).

[15] E. K. Ko, Y. Yu, Y. Liu, L. Bhatt, J. Li, V. Thampy, C.-T. Kuo, B. Y. Wang, Y. Lee, K. Lee *et al.*, *Signatures of ambient pressure superconductivity in thin film* $La_3Ni_2O_7$, Nature (London) **638**, 935 (2025).

[16] F. Li, Z. Xing, D. Peng, J. Dou, N. Guo, L. Ma, Y. Zhang, L. Wang, J. Luo, J. Yang *et al.*, *Ambient pressure growth of bilayer nickelate single crystals with superconductivity over 90 K under high pressure*, Nature (London) **649**, 871 (2025).

[17] E. Zhang, D. Peng, Y. Zhu, L. Chen, B. Cui, X. Wang, W. Wang, Q. Zeng, and J. Zhao, *Bulk superconductivity in pressurized trilayer nickelate* $Pr_4Ni_3O_{10}$ *single crystals*, Phys. Rev. X **15**, 021008 (2025).

[18] M. Rossi, M. Osada, J. Choi, S. Agrestini, D. Jost, Y. Lee, H. Lu, B. Y. Wang, K. Lee, A. Nag *et al.*, *A broken translational symmetry state in an infinite-layer nickelate*, Nat. Phys. **18**, 869 (2022).

[19] G. Krieger, L. Martinelli, S. Zeng, L. E. Chow, K. Kummer, R. Arpaia, M. Moretti Sala, N. B. Brookes, A. Ariando, N. Viart, M. Salluzzo, G. Ghiringhelli, and D. Preziosi, *Charge and spin order dichotomy in* $NdNiO_2$ *driven by the capping layer*, Phys. Rev. Lett. **129**, 027002 (2022).

[20] C. C. Tam, J. Choi, X. Ding, S. Agrestini, A. Nag, M. Wu, B. Huang, H. Luo, P. Gao, M. García-Fernández *et al.*, *Charge density waves in infinite-layer* $NdNiO_2$ *nickelates*, Nat. Mater. **21**, 1116 (2022).

[21] C. T. Parzyck, N. K. Gupta, Y. Wu, V. Anil, L. Bhatt, M. Bouliane, R. Gong, B. Gregory, A. Luo, R. Sutarto *et al.*, *Absence of* $3a_0$ *charge density wave order in the infinite-layer nickelate* $NdNiO_2$, Nat. Mater. **23**, 486 (2024).

[22] J. Zhang, Y.-S. Chen, D. Phelan, H. Zheng, M. R. Norman, and J. F. Mitchell, *Stacked charge stripes in the quasi-2D trilayer nickelate* $La_4Ni_3O_8$, Proc. Natl. Acad. Sci. U.S.A. **113**, 8945 (2016).

[23] T. Xie, M. Huo, X. Ni, F. Shen, X. Huang, H. Sun, H. C. Walker, D. Adroja, D. Yu, B. Shen, L. He, K. Cao, and M. Wang, *Strong interlayer magnetic exchange coupling in* $La_3Ni_2O_{7-\delta}$ *revealed by inelastic neutron scattering*, Sci. Bull. **69**, 3221 (2024).

[24] R. Khasanov, T. J. Hicken, D. J. Gawryluk, V. Sazgari, I. Plokhikh, L. P. Sorel, M. Bartkowiak, S. Bötzel, F. Lechermann, I. M. Eremin, H. Luetkens, and Z. Guguchia, *Pressure-enhanced splitting of density wave transitions in* $La_3Ni_2O_{7-\delta}$, Nat. Phys. **21**, 430 (2025).

[25] J. Zhang, D. Phelan, A. Botana, Y.-S. Chen, H. Zheng, M. Krogstad, S. G. Wang, Y. Qiu, J. Rodriguez-Rivera, R. Osborn *et al.*, *Intertwined density waves in a metallic nickelate*, Nat. Commun. **11**, 6003 (2020).

[26] A. M. Samarakoon, J. Strempfer, J. Zhang, F. Ye, Y. Qiu, J.-W. Kim, H. Zheng, S. Rosenkranz, M. R. Norman, J. F. Mitchell, and D. Phelan, *Bootstrapped dimensional crossover of a spin density wave*, Phys. Rev. X **13**, 041018 (2023).

[27] J. Zhang, H. Zheng, Y.-S. Chen, Y. Ren, M. Yonemura, A. Huq, and J. F. Mitchell, *High oxygen pressure floating zone growth and crystal structure of the metallic nickelates* $R_4Ni_3O_{10}$ *(*R = La*,* Pr*)*, Phys. Rev. Mater. **4**, 083402 (2020).

[28] J. Tranquada, B. Sternlieb, J. Axe, Y. Nakamura, and S.-i. Uchida, *Evidence for stripe correlations of spins and holes in copper oxide superconductors*, Nature (London) **375**, 561 (1995).

[29] C. H. Chen, S. W. Cheong, and A. S. Cooper, *Charge modulations in* $La_{2-x}Sr_xNiO_{4+y}$*: Ordering of polarons*, Phys. Rev. Lett. **71**, 2461 (1993).

[30] J. Mitchell, D. Argyriou, A. Berger, K. Gray, R. Osborn, and U. Welp, *Spin, charge, and lattice states in layered magnetoresistive oxides*, J. Phys. Chem. B **105**, 10731 (2001).

[31] See Supplemental Material at http://link.aps.org/supplemental/10.1103/s5j9-cbg7, for additional data and analyses about XRD, energy resolution of IXS measurements, phonon spectra around CDW wave vector and SDW wave vector in $Pr_4Ni_3O_{10}$ and phonon spectra around CDW wave vector in $La_4Ni_3O_{10}$.

[32] A. H. Said, H. Sinn, T. S. Toellner, E. E. Alp, T. Gog, B. M. Leu, S. Bean, and A. Alatas, *High-energy-resolution inelastic X-ray scattering spectrometer at beamline 30-ID of the Advanced Photon Source*, J. Synchrotron Radiat. **27**, 827 (2020).

[33] M. R. Norman, *Landau theory of the density wave transition in trilayer Ruddlesden-Popper nickelates*, Phys. Rev. B **112**, 075149 (2025).

[34] E. Fawcett, *Spin-density-wave antiferromagnetism in chromium*, Rev. Mod. Phys. **60**, 209 (1988).

[35] J. M. Tranquada, K. Nakajima, M. Braden, L. Pintschovius, and R. J. McQueeney, *Bond-stretching-phonon anomalies in stripe-ordered* $La_{1.69}Sr_{0.31}NiO_4$, Phys. Rev. Lett. **88**, 075505 (2002).

[36] A. Merritt, A. Christianson, A. Banerjee, G. Gu, A. Mishchenko, and D. Reznik, *Giant electron–phonon coupling of the breathing plane oxygen phonons in the dynamic stripe phase of* $La_{1.67}Sr_{0.33}NiO_4$, Sci. Rep. **10**, 11426 (2020).

[37] R. P. Gupta and A. J. Freeman, *Role of matrix elements in the theoretical determination of generalized susceptibilities in metals*, Phys. Rev. B **13**, 4376 (1976).

[38] D. Lamago, M. Hoesch, M. Krisch, R. Heid, K.-P. Bohnen, P. Böni, and D. Reznik, *Measurement of strong phonon softening in Cr with and without fermi-surface nesting by inelastic X-ray scattering*, Phys. Rev. B **82**, 195121 (2010).

[39] F. Weber, S. Rosenkranz, J.-P. Castellan, R. Osborn, R. Hott, R. Heid, K.-P. Bohnen, T. Egami, A. H. Said, and D. Reznik, *Extended phonon collapse and the origin of the charge-density wave in* $2H\text{-}NbSe_2$, Phys. Rev. Lett. **107**, 107403 (2011).

[40] J. Zhang, A. Botana, J. Freeland, D. Phelan, H. Zheng, V. Pardo, M. Norman, and J. Mitchell, *Large orbital polarization in a metallic square-planar nickelate*, Nat. Phys. **13**, 864 (2017).

[41] G. Kresse and J. Hafner, *Ab initio molecular dynamics for liquid metals*, Phys. Rev. B **47**, 558 (1993).

[42] G. Kresse and J. Furthmüller, *Efficient iterative schemes for ab initio total-energy calculations using a plane-wave basis set*, Phys. Rev. B **54**, 11169 (1996).

[43] J. P. Perdew, K. Burke, and M. Ernzerhof, *Generalized gradient approximation made simple*, Phys. Rev. Lett. **77**, 3865 (1996).

[44] P. Blaha, K. Schwarz, F. Tran, R. Laskowski, G. K. H. Madsen, and L. D. Marks, *WIEN2K: An* APW + lo *program for calculating the properties of solids*, J. Chem. Phys. **152**, 074101 (2020).

[45] D. D. Koelling and J. H. Wood, *On the interpolation of eigenvalues and a resultant integration scheme*, J. Comput. Phys. **67**, 253 (1986).

[46] J. Rath and A. J. Freeman, *Generalized magnetic susceptibilities in metals: Application of the analytic tetrahedron linear energy method to Sc*, Phys. Rev. B **11**, 2109 (1975).